Winter mass balance of Drangajökull ice cap (NW Iceland) derived from satellite sub-meter stereo images

Joaquín M. C. Belart[1,2], Etienne Berthier[2], Eyjólfur Magnússon[1], Leif S. Anderson[1], Finnur Pálsson[1], Thorsteinn Thorsteinsson[3], Ian Howat[4], Guðfinna Aðalgeirsdóttir[1], Tómas Jóhannesson[3], Alexander H. Jarosch[1]

[1]Institute of Earth Sciences, University of Iceland, Askja, Reykjavík, Iceland
[2]Laboratoire d'Etudes en Géophysique et Océanographie Spatiales, Centre National de la Recherche Scientifique (LEGOS – CNRS), Université de Toulouse, Toulouse, France
[3]Icelandic Meteorological Office, Reykjavík, Iceland
[4]School of Earth Sciences and Byrd Polar and Climate Research Center, Ohio State University, Columbus, USA

Correspondence to: Joaquín M.C. Belart (jmm11@hi.is)

Abstract. Sub-meter resolution satellite stereo images allow the generation of high resolution, accurate digital elevation models (DEMs). Repeated acquisitions of stereo images from Pléiades, in October 2014 and May 2015, and from WorldView2 (WV2), in February 2015, over Drangajökull ice cap (NW-Iceland) are used to estimate the geodetic glacier-wide mass balance on sub-annual time scales. Relative adjustment of the DEMs is performed with and without a pre-existing lidar DEM as source of ground control points (GCPs), and resulting statistics in snow-free and ice-free areas reveal similar vertical accuracy <0.5 m for both methods. The estimated accuracy of the average elevation change from October to May, without using lidar GCPs, was 0.22 m, showing the capabilities of the satellites for measuring snow accumulation in a seasonal time span without external data. The winter mass balance of Drangajökull is $B_w = 3.20 \pm 0.21$ m w.e during October-May, and ~60% of the accumulation occurred during October-February, a percentage in good agreement with the precipitation record at a nearby meteorological station. The elevation change from October to May was compared with winter snow thickness measured at 8 locations in June 2015. Winter snow of 6.5 m was measured in the cores on average while the DEM difference shows average elevation change of 5.1 m at the same locations. This systematic difference is explained by (1) difference in time between in situ and satellite observations, (2) firn compaction and (3) elevation change due to ice dynamics. This study demonstrates that seasonal geodetic mass balance can in many areas be measured from sub-meter resolution satellite stereo images, as a complement or even replacement of in situ measurements.

1 Introduction

Continuous monitoring of glacier change enables understanding of the close connection between glacier mass balance and climate change (Vaughan et al., 2013). This monitoring is based on in situ and remote sensing measurements, and has confirmed the strong sensitivity of glaciers to climate change and a continuous retreating and mass wastage in most of the glaciated regions in the world (Vaughan et al., 2013; Zemp et al., 2015).

However seasonal (end of winter accumulation and summer ablation) records of glacier changes are sparse (Ohmura, 2011). Measurements are lacking in many glaciated areas due to high cost and the logistical challenges, despite they contain valuable information for the short term overview of mass budget and its implications for water storage, runoff and regional climate (e.g. Huss et al., 2008). These measurements are also helpful for revealing the trends and patterns in changes of glaciers and for

5   improving glacier models (e.g. Huss et al., 2008; Adalgeirsdóttir et al., 2011).

The most widely-used and trusted technique for measuring the winter accumulation is based on in situ measurements, e.g. snow probing, snow pits and/or shallow cores. With an adequate spatial sampling this method measures glacier-wide mass balance with errors of 0.1 to 0.3 m w.e. (Ohmura, 2011). Remote sensing-based methods have been occasionally used for measuring snow accumulation, such as repeated lidar surveys (e.g. Sold et al., 2013; Helfricht et al., 2014) or unmanned aerial

10 vehicles (UAVs) surveys (Bühler et al., 2016; De Michele et al., 2016) which allow creation of highly accurate and detailed DEMs that are compared for measuring changes in elevation and volume due to snow accumulation.

Satellite stereo images with sub-meter resolution (e.g. from WorldView or Pléiades) are used for the creation of accurate, detailed DEMs, with access to any remote area of the world. The imaged glaciated areas show typically adequate contrast and mostly no saturation even in bright and featureless snow areas (e.g. Berthier et al., 2014; Holzer et al., 2015; Willis et al.,

15 2015). The DEMs obtained from these sensors have been tested and assessed in numerous studies (e.g. Berthier et al., 2014; Howat et al., 2015; Lacroix et al., 2015; Willis et al., 2015), reporting relative DEM accuracy ranging 0.2 m to 1 m (Berthier et al., 2014; Lacroix et al., 2015; Noh and Howat, 2015). This indicates the high potential of these sensors for measuring changes over short spans of time in glaciers with adequate mass turnover. Sequential Pléiades DEMs have recently been successfully used for measuring snowfall in mountainous areas (Marti et al., 2016).

20 This paper is focused on testing the capabilities of Pléiades and WV2 DEMs for measuring winter snow accumulation over an Icelandic ice cap. A processing chain is developed for constructing co-registered DEMs from sub-meter resolution optical stereo images. The methodology does not require external reference data and could be applied in most glaciated areas. The spaceborne results are validated with in situ measurements of snow accumulation.

2 Study site and data

25 ### 2.1 Drangajökull ice cap

Iceland has about 11000 km^2 of its land covered by glaciers (Björnsson and Pálsson, 2008). Glaciological mass balance studies have been conducted on the three largest ice caps: Vatnajökull (since 1991, Björnsson et al., 2013), Langjökull (since 1997, Pálsson et al., 2012) and Hofsjökull (since 1988, Jóhannesson et al., 2013) (Fig. 1).They have contributed to the knowledge of the impacts of climate change on glacier variations in the North Atlantic and the results are important for the use of glacier

30 meltwater in hydropower plants.

Field campaigns are carried out twice per year for recording the winter accumulation and summer ablation at selected locations (Björnsson and Pálsson, 2008; Björnsson et al., 2013). Icelandic glaciers have a high mass turnover, typically ~2 m w.e. for

the monitored ice caps (Pálsson et al., 2012; Björnsson et al., 2013). The turnover is expected to be even higher in other glaciated areas such as Mýrdalsjökull and Öræfajökull ice caps (S-Iceland) where limited mass balance surveys in the accumulation area have repeatedly shown winter accumulation of 5-7 m w.e. (Guðmundsson, 2000; Ágústsson et al., 2013).

Our study area is Drangajökull ice cap, located in NW Iceland (Fig. 1). It spans an elevation from ~60 m to ~900 m a.s.l and an area of 143 km^2 (in 2014). Its climatic situation is substantially different from other Icelandic glaciers located closer to the southern coasts or in the central part of the island (Jóhannesson et al., 2013; Magnússon et al., 2016). Geodetic observations have revealed that the average Drangajökull glacier-wide mass balance during the period 1946-2011 was moderately negative at -0.26±0.04 m w.e.a^{-1} (Magnússon et al., 2016). The same observations revealed a striking difference in the mass balance between the western and eastern sides of the ice cap during this period, corresponding to -0.16 ± 0.05 m w.e.a^{-1} and -0.41 ± 0.04 m w.e.a^{-1}, respectively. The spatial distribution of the winter snow accumulation is likely to explain part of this trend.

The relatively recent records of in situ mass balance measurements on this ice cap, together with the expected amount of snow accumulation of several meters during the winter, make Drangajökull ice cap an interesting study site for developing the described remote sensing methods. The size of Drangajökull makes it ideal for testing Pléiades and WV stereo images, which can cover the ice cap entirely or nearly entirely with a single stereo pair.

2.2 Satellite stereo images

Two pairs of Pléiades (French Space Agency, CNES) stereo images were scheduled and acquired over Drangajökull ice cap, the first on 14 October 2014, the beginning of the winter 2014-2015 and the later on 22 May 2015, at the end of the same winter (Table 1 and Fig. 2). The Pléiades sensor has a swath of 20 km, which allowed covering the entire ice cap and its vicinity in a single scene. The rational polynomial coefficients (RPCs) for the sensor model were also provided.

An additional dataset was obtained from WV2 (DigitalGlobe Inc via the U.S. National Geospatial Intelligence Agency) stereo images, acquired on 13 February 2015, covering ~92% of the ice cap (Table 1 and Fig. 2). This dataset was collected and processed as part of the ongoing U.S. National Science Foundation ArcticDEM project. A DEM with 2 m resolution was produced with the Surface Extraction with TIN-based Search-space Minimization (SETSM) software (Noh and Howat, 2015), using the RPC sensor model and no GCPs. WV2 orthoimages were also provided in 2 m resolution.

Pléiades and WV2 images have a spatial resolution of 0.7 m and 0.5 m at nadir, respectively. The images are encoded in 12 bits (Pléiades) and 11 bits (WV2). The base to height (B/H) ratio from the stereo pairs ranges between 0.4 and 0.5 (table 1), providing a good geometry of stereoscopy without compromising the coverage of the DEMs in steep areas.

The Pleiades images from October 2014 were acquired one day after the first significant snowfall of the winter (Fig. 2), showing fresh snow covering most of the imaged area. All the fine details of the bare terrain can, however, be clearly observed in the images, including small boulders and other features of the bare ground.

Due to the low solar angle, the October 2014 and February 2015 images contain large shadows north of cliffs and nunataks, causing lack of contrast in these areas. The images of May 2015 contain areas with clouds in the southern border of

Drangajökull, mostly located off-glacier (Fig. 2), and few thin clouds over the ice cap although the glacier surface remains visible. The orthoimage of February 2015 reveals a similar snow extent off-glacier as the images of May 2015.

2.3 Lidar

A lidar DEM was produced from an airborne survey in July 2011 (Fig. 1), part of larger effort to survey all Icelandic glaciers
5 and ice caps between years 2008-2012 (Jóhannesson et al., 2013). For Drangajökull, this survey covered an extensive ice-free area outside the ice cap, up to ~10 km in some locations. The survey was carried out with a lidar sensor model Optech ALTM 3100, with a typical point cloud density of 0.33 pts/m^2. From the point cloud a 2 x 2 m grid was produced (Magnússon et al., 2016). An uncertainty assessment was previously carried out for another lidar dataset from the same sensor acquired in similar conditions, revealing an absolute vertical accuracy better than 0.5 m (Jóhannesson et al., 2011).

10 ## 2.4 In situ and meteorological measurements

Measurements of winter snow thickness and density have been carried out by the Icelandic Meteorological Office (IMO) and the National Energy Authority on Drangajökull since 2005. Snow cores have been drilled at 6-8 locations at the end of each winter (except 2013), yielding the winter mass balance at each location. Five points were added during a campaign organized by the Institute of Earth Sciences (IES), University of Iceland in spring 2014 (Fig. 1).
15 The in situ data from 8 of these locations is used in this work, as measured by IMO in the spring of 2015. These measurements were carried on 19 June 2015, one month later than usual, due to unusually cool conditions in the spring. All available in situ records of snow density from 2005-2014 were also used in this study.
A map of in situ net mass balance was also used, obtained during the glaciological year 2013-2014 (unpublished data, IMO and IES) from a combination of mass balance point measurements and profiles of snow depth from ground penetrating radar
20 (GPR).
Precipitation and temperature data from the meteorological station Litla-Ávík (40 km SE of Drangajökull, 15 m a.s.l. Fig. 1) were compiled from IMO, in daily records for the entire years 2014-2015.

3 Methods

3.1 Processing of satellite data

25 The WV2 DEM and ortho-image were directly provided through the ArcticDEM project. The two pairs of Pléiades stereo images were processed in order to produce the respective DEMs and orthoimages. The three DEMs need to be co-registered horizontally and vertically for accurate and unbiased volume change estimates (e.g. Nuth and Kääb, 2011).
Two different workflows were tested for obtaining co-registered DEMs (Fig. 3): scheme A uses lidar-based GCPs as a reference, whereas scheme B uses common snow-free and ice-free areas between the datasets. Statistics of the snow-and ice-
30 free areas with both schemes indicates whether there is a significant added value of using external reference data in the DEM

processing, such as lidar-based GCPs. Due to the lack of raw images, the only methodology carried out for the WV2 DEM co-registration was scheme B (Fig. 3).

Each scheme results in co-registered DEMs with 4 x 4 m cell size, and orthoimages with 0.5 x 0.5 m pixel size. The spatial resolution of the created DEMs and orthoimages is considered adequate for measurements of snow, and represents a good

5 compromise between the processing time and usefulness of the images (Marti et al., 2016).

3.1.1 Scheme A: Processing of Pléiades data using lidar-derived GCPs

The shaded relief lidar DEM was used as reference for extracting GCPs, in a similar approach as described by Berthier et al. (2014). The GCPs were typically boulders easily recognized from both the lidar hillshade and the stereo images, adequately spread horizontally and vertically around the whole study area (Nuth and Kääb, 2011). Each pair of Pléiades stereo images

10 was processed separately using the software ERDAS Imagine (© Intergraph). 40 tie points (TPs) were automatically measured on each stereo pair, and 10 GCPs were manually digitized, five of which are common in the October 2014 and May 2015 images. The original RPCs from the images were thus refined by including the GCPs and TPs in the bundle adjustment.

After the RPCs refinement, a DEM was produced from stereo pair by using pixelwise stereo-matching with the routine enhanced Automatic Terrain Extraction (eATE), using the images resampled to twice the raw pixel size (pyramid level 1),

15 which gives an adequate compromise between the speed of processing and DEM quality. The obtained point clouds were linearly interpolated into gridded DEMs. The orthoimages were produced from the most nadir image of each pair.

Lidar-based GCPs from ice-free areas have been repeatedly used in photogrammetric studies on glaciers (e.g. James et al., 2006; Berthier et al., 2014; Magnússon et al., 2016). With present-day satellite data, a few GCPs are sufficient to remove most of the horizontal and vertical biases in the resulting optical DEMs (Berthier et al., 2014; Shean et al., 2016).

20 ### 3.1.2 Scheme B: Processing of Pléiades data with DEM co-registration

In this approach, the DEMs were produced from the pair of stereo images with only the original RPCs. This work was carried out with the open source software Ames StereoPipeline (ASP, version 2.5.2) developed by NASA (Shean et al., 2016). The processing chain uses the routine *stereo*, producing a point cloud from each pair of stereo images, followed by the routine *point2dem*, which produces the gridded DEM and the orthoimage for each pair of stereo images. Further detail of these routines

25 is described by Shean et al. (2016).

Areas with sparse cloud coverage from the May 2015 images were processed separately, and mosaicked and superimposed over the initial DEM and orthoimage. The correlation performed in this areas was based directly on the full-resolution images, instead of a gradual correlation from sub-sample images. This improved the correlation in the identified low-contrast areas (Shean et al., 2016).

30 The resulting DEMs and orthoimages contained a visible offset in the horizontal and vertical positioning as well as a planar tilt. To correct this bias, the routine *pc_align* was applied in ASP software, using the Iterative Closest Point (ICP) algorithm for co-registration of two point clouds (Pomerleau et al., 2013). The ICP algorithm applied was performed in two runs: (1) the

snow-free and ice-free areas of the May 2015 DEM were used as a slave DEM, and the entire October 2014 DEM was used as a master DEM, calculating a transformation matrix with 7 parameters (3 rotations, 3 translations and a scale factor) between the two DEMs. (2) The calculated transformation was applied to the entire May 2015 DEM. The applied transformation was equivalent to a global translation of -4.50 m in Northing, -3.95 m in Easting and 0.29 m in vertical component of the original

5   DEM. A planar tilt of 0.03° between the two DEMs was also corrected in this process.

3.1.3 Co-registration of the WV2 DEM

The WV2 February 2015 DEM was co-registered to the October 2014 DEM (scheme B), by using the ICP algorithm as described in the previous section. The original 2 x 2 m WV2 DEM was bilinearly resampled to 4 x 4m. The ICP algorithm was applied to the ice-free areas in May 2015 after verifying similar distribution of snow-free areas between the orthoimages of

10 February and May 2015. The coregistered WV2 DEM had an equivalent translation of -3.25 m in Northing, 3.31 m in Easting and -5.44 m in vertical component, relative to the original DEM, as well as a correction for planar tilt of 0.02°.

3.1.4 Statistics in snow-free and ice-free areas

The bare ground areas from May 2015 (Fig. 2) were used for comparison of the DEMs for uncertainty analysis. This assumed a negligible amount of snow off-glacier in the images of October 2014, quantified on average less than 20 cm outside the

15 glacier and further reduced at boulders and topographic highs generally used as GCPs (further described in section 3.4.1). For delineating the snow-free and ice-free areas, the May 2015 orthoimage was binarized by setting up a cutoff value of 819 out of the 4095 digital numbers (DN) of the image. These images show clear contrast between snow and bare ground (Fig. 2), making image segmentation an efficient approach to identify the bare ground.

Statistical indicators of bias and data dispersion were calculated from the difference of DEMs (dDEM) in snow-free and ice-

20 free areas, using the October 2014 DEM as a reference. This included number of cells over snow-free and ice-free terrain, median, mean, standard deviation (SD) and normalized median absolute deviation (NMAD, Höhle and Höhle, 2009). The statistical analysis was also carried out with filtered elevation difference in snow-free and ice-free areas, after masking out high slope areas and shadow-covered areas. These are expected to contain higher level of noise and appearing in a negligible amount over the ice cap. All snow-free and ice-free areas with slopes >20° were masked out, as performed in previous similar

25 studies (Magnússon et al., 2016). Shadows of the October 2014 and February 2015 DEMs were masked out from analytical hillshading (Tarini et al., 2006), using the sun position at the time of acquisition for the respective images.

DEM uncertainty based on SD or NMAD conservatively assumes totally correlated errors in the dDEM (Rolstad et al., 2009). However the spatial autocorrelation inherent in the DEM may produce substantially lower uncertainty estimates than calculated by simple statistics (Rolstad et al., 2009; Magnússon et al., 2016). A sequential Gaussian simulation (SGSim) was performed

30 over the masked snow-free and ice-free areas (Magnússon et al., 2016), in order to calculate a likely bias-corrected mean elevation difference inside the ice cap and its associated standard deviation.

3.2 Computation of glacier-wide mass balance

Three dDEMs were produced from the different combinations: $dDEM_{t1}^{t2}$, $dDEM_{t2}^{t3}$ and $dDEM_{t1}^{t3}$, where t_1 = 14 October 2014; t_2 = 13 February 2015; and t_3 = 22 May 2015. The geodetic mass balance was calculated using the following equation:

$$B_{t_i}^{t_f} = \rho_{snow} \left(\bar{h}_{dDEM_{t_i}^{t_f}} + \overline{ch}_{Firn_{t_i}^{t_f}} \right), \tag{1}$$

Where t_i and t_f are the dates of the first and last DEMs used, respectively. ρ_{snow} represents the density of the snow. $\bar{h}_{dDEM}$ is the average elevation change over the ice cap obtained from dDEM, and $\overline{ch}_{Firn}$ is the average elevation correction due to firn compaction over the entire ice cap. Assuming the variables of (Eq. 1) are uncorrelated to one another, the error in the mass balance calculation is obtained by:

$$\Delta B = \sqrt{\left(\frac{\partial B}{\partial \rho_{snow}} \Delta_{\rho_{snow}} \right)^2 + \left(\frac{\partial B}{\partial \bar{h}_{dDEM}} \Delta_{\bar{h}_{dDEM}} \right)^2 + \left(\frac{\partial B}{\partial \bar{h}_{Firn}} \Delta_{\overline{ch}_{Firn}} \right)^2}$$

$$= \sqrt{\left(\left(\bar{h}_{dDEM} + \overline{ch}_{Firn} \right) \Delta_{\rho_{snow}} \right)^2 + \left(\rho_{snow} \Delta_{\bar{h}_{dDEM}} \right)^2 + \left(\rho_{snow} \Delta_{\overline{ch}_{Firn}} \right)^2}, \tag{2}$$

Where $\Delta_{\bar{h}_{dDEM}}$ is the uncertainty in average elevation change obtained from dDEM, $\Delta_{\overline{ch}_{Firn}}$ is the uncertainty in firn correction and $\Delta_{\rho_{snow}}$ is the uncertainty in snow density used.

The data gaps in the dDEMs inside the ice cap occur in areas of large shadows north of the nunataks, in October 2014 and in February 2015, and due to the extent of the scenes in February 2015 where the south-easternmost part of the ice cap is missing (Fig. 1 and 2). This lead to <1% of data gaps for $dDEM_{t1}^{t3}$, and ~8% of data gaps for $dDEM_{t1}^{t2}$ and $dDEM_{t2}^{t3}$. The gaps on $dDEM_{t1}^{t3}$ were filled by interpolation of the average elevation difference at the surrounding locations. These gaps have virtually no effect on the glacier-wide mass balance calculation. The gaps of $dDEM_{t1}^{t2}$ and $dDEM_{t2}^{t3}$ were filled by assuming a linear relation between the average elevation difference at the overlapping areas (~92% of total area) of $dDEM_{t1}^{t3}$ with $dDEM_{t1}^{t2}$ and $dDEM_{t2}^{t3}$ respectively. This allowed a linear extrapolation of the total elevation difference of $dDEM_{t1}^{t3}$ into the total elevation difference of $dDEM_{t1}^{t2}$ and $dDEM_{t2}^{t3}$.

The area extent of the ice cap was digitized from the orthoimage of October 2014, following the criteria defined in Magnússon et al. (2016) for glacier delineation, which excludes snowfields located at the eastern and southern sides of the glacier. Uncertainties caused by glacier digitation are neglected in this study due to the high resolution of images and its low impact on the volume calculations.

3.2.1 Firn densification

Compaction of the firn layer produces a continuous surface lowering of the glacier accumulation area. This is not taken into account when looking at the elevation difference from dDEM, resulting in an underestimation of snow accumulation (Sold et al., 2013). The total area covered by firn at the end of the 2014 ablation season was 91km^2, or about 64% of the ice cap, based

on observations of a Landsat 8 image acquired 16 September 2014 (data available from the U.S. Geological Survey, http://earthexplorer.usgs.gov/). This is in reasonable agreement with the map of net annual mass balance of the year 2013-2014 deduced from in situ measurements, showing 58% of the glacier area with positive mass balance at the end of the summer. The net mass balance distribution of the year 2013-2014 was used to correct for firn densification, assuming that this represents

5 an average year of mass balance for Drangajökull. The net annual elevation change due to firn compaction integrated over the entire firn column should correspond to the average annual accumulation layer transformed from snow to ice during one glaciological year (Sold et al., 2013), and is calculated as follow:

$$ch_{Firn} = \frac{b_{n+}}{\rho_u} - \frac{b_{n+}}{\rho_l}, \tag{3}$$

Where b_{n+} is the positive mass balance of 2013-2014 over the firn areas, and ρ_u and ρ_l are the upper and lower values of

10 density of the firn profile, estimated as $\rho_u = 600$ kg/m^3 and $\rho_l = 900$ kg/m^3. These values of density in the firn layer are consistent with the literature (Cuffey and Paterson, 2010) and with a measured deep density profile obtained on Hofsjökull ice cap in central Iceland (Thorsteinsson et al., 2002). Assuming that the firn compaction rate does not vary seasonally, the annual firn   compaction   was   distributed   linearly   over   the   time   span   covered   (0.603   years   for t_1^3 and 0.334 years for t_1^2).

15 The firn compaction correction maps were added to $dDEM_{t1}^{t3}$ and $dDEM_{t1}^{t2}$ before calculating the geodetic mass balance. On average, this caused a correction in firn areas of 0.41 m and 0.23 m for t_1^3 and t_1^2 respectively, resulting in a glacier-wide correction of $\overline{ch}_{Firn_{t_1}^{t_3}} = 0.24$ m and $\overline{ch}_{Firn_{t_1}^{t_2}} = 0.13$ m.

The quantification of the firn compaction is based on the assumption that equal amount of net accumulation occurs every year, as well as a constant compaction rate through a glaciological year. It is therefore expected that these assumptions will result in

20 uncertainties in this correction, which propagate through (Eq. 3). We assign an uncertainty of 50% of the total firn correction to the error budget during the uncertainty assessment in the mass balance calculations (Table 3).

3.2.2 Density of snow

The average density of winter snow on Drangajökull at the end of the winter 2015 was ρ = 554 kg/m^3, as deduced from the measurements of the 8 snow cores at elevations ranging from 300-920 m. This value is used for conversion of volume to water

25 equivalent for the geodetic mass balance calculation from $dDEM_{t1}^{t3}$. The estimated uncertainty in snow density is ± 27 kg/m^3, obtained from the year to year and point to point variations of the snow density. This error should cover the uncertainty in density caused by (1) errors in measurements and (2) likely snow densification between the May 2015 Pléiades images and the June 2015 field campaign.

The density of new snowfall for the first half of the winter is expected to be lower than the total snow density measured at the

30 end of the winter. The value 500 kg/m^3 was used for the mass balance calculations from $dDEM_{t1}^{t2}$. This lower value of density has been observed in a few occasions on Drangajökull at early spring measurements (Fig. 7). The uncertainty assigned to this density is ± 50 kg/m^3.

Instead of assigning a density value for the calculation of the mass balance using $dDEM_{t2}^{t3}$, B_{t2}^{t3} was calculated as the difference between the total B_{t1}^{t3} and B_{t1}^{t2}. The error budget for B_{t2}^{t3} was calculated as the quadratic component of the errors of B_{t1}^{t3} and B_{t1}^{t2}.

3.3 Comparison of Pléiades-based elevation changes and in situ measurements

5 The elevation difference obtained from $dDEM_{t1}^{t3}$ was compared with the snow thickness measured at the in situ locations. Three main factors cause differences in results between the remote sensing and the glaciological method (Sold et al., 2013): (1) the difference in time between the DEMs and in situ surveys, (2) the compaction of firn and (3) the surface emergence and submergence due to ice dynamics. The corrected satellite-based elevation difference $CdDEM_{t1}^{t3}$ for comparison to in situ data is calculated as:

10 $$CdDEM_{t1}^{t3} = dDEM_{t1}^{t3} + cht_{Oct} + cht_{May\&Jun} + ch_{Firn} + ch_{Ice\ dyn.} \tag{4}$$

Where cht_{Oct} and $cht_{May\&Jun}$ are corrections of elevation due to snowfalls and melt events between image acquisitions and in situ measurements (section 3.3.1), ch_{Firn} is the correction of elevation due to firn compaction (section 3.3.2) and $ch_{Ice\ dyn.}$ is the surface emergence and submergence due to ice dynamics (section 3.3.3). The magnitude/sign of these corrections differ between the accumulation and ablation areas (Fig. 4).

15 ### 3.3.1 Difference in time between in situ and Pléiades dDEM

There is a mismatch in time between the in situ measurements, obtained on the 19 June 2015 and measuring the thickness of snow that fell since early October, rough date of the formation of the firn layer marking the end of the previous summer, and the Pléiades stereo images, measuring the elevation changes between 14 October 2014 and 22 May 2015 (Fig. 5). To estimate the amount of snow that fell or melted outside the overlapping period, a first inspection was done on satellite images acquired

20 by the moderate resolution imaging spectroradiometer (MODIS) and Landsat 8 in September, October 2014, May and June 2015.

From the MODIS and Landsat images, the first snowfall of the winter was detected on the 3 October 2014. This snow melted away in the ice-free areas in the consecutive days. A second snowfall occurred on the 13 October 2014. After the acquisition of the May 2015 Pléiades stereo pair, a snowfall was observed the 28 and 29 May 2015. Melting events were also observed

25 during the last part of the winter, prior to the in situ survey.

To quantify the effect of the snow accumulation and melting in the in situ/satellite elevation difference, the daily precipitation and temperature records were used from the manned weather station at Litla-Ávík (Fig. 5). The meteorological station recorded a net precipitation of 684 mm between the 1 October 2014 and the 19 June 2015. The recorded total winter precipitation and the in situ winter mass balance measurements allowed calculation of a scaling factor between the precipitation values at the

30 meteorological station and at the location of each in situ point. The scaling factor varies significantly between each in situ location, between factor ~2 and factor ~7, indicating a non-uniform distribution of precipitation on the glacier. The temperature

recorded at the meteorological station was also translated into temperature at each in situ location, by applying an elevation lapse rate of -6° km^{-1} (Guðmundsson et al., 2009).

All the precipitation events with temperatures <1° are assumed to be snowfalls. The total amount of precipitation for temperatures <1° was on average 60 mm for the period 1-14 October 2014, and 43 mm for the period 22 May to 19 June 2015.

5 This precipitation was scaled and converted to snow with a density of 400 kg/m^3, using the typical density value for newly fallen snow on ice caps in Iceland.

The scaled precipitation at locations V1, V2 and V5 (the closest in situ locations to the ice-free areas) was also used to quantify the amount of snow fallen on the ice-free areas prior to the October Pléiades acquisition, assuming a snow density of 400 kg/m^3. This yielded a minimum estimated snowfall of 0.15 m at V1 (291 m a.s.l.) and a maximum of 0.30 m at V2 (668 m

10 a.s.l.). The snow line was observed to lie at an elevation of ~50 m a.s.l. during this time. The snow layer in ice-free areas is therefore expected to be less than 20 cm, considering its elevation range.

The melting events outside the overlapping periods were also estimated from a simple positive degree-day melting model. The model uses a degree day melt factor, ddf, of 5.5 mm w.e. °C^{-1}, obtained for snow on Langjökull ice cap (central Iceland) (Guðmundsson et al., 2009). Positive degree days were summed for days with temperature above 0° and the density of melted

15 snow was assumed to be 500 kg/m^3. Melting amounted to a maximum of 0.40 m in October 2014 (V2) and 1.08 m in May-June 2015 (V1).

3.3.2 Firn compaction

This process has been explained in section 3.3.1 and it affects also the comparison between geodetic and glaciological methods (Fig. 4). Using (Eq. 3) the firn compaction was calculated for the in situ locations with positive mass balance, points V3, V4,

20 V6, V7 and J2. The maximum firn compaction correction was 0.53 m at the in situ location V3, which presented a net mass balance of 1.73 m w.e. during the year 2013-2014.

3.3.3 Ice dynamics

In order to estimate the effect of the ice dynamics on local surface elevation change during the study period, two approaches were considered based on the literature and previous case-studies (e.g. Jarosch, 2008; Sold et al., 2013):

25   1) The emergence velocities were calculated using a Stokes ice flow model. The Icetools library (Jarosch, 2008) was run with the finite element package, Fenics. The model calculates a 3D velocity field resulting from the ice deformation, given the glacier geometry. Bedrock DEM (unpublished data of IES, based on ~600 km of low frequency radar profiles evenly distributed over the whole glacier) and glacier surface DEM from October 2014 were used as input. The 2D horizontal velocities measured from GPS in the 2013-2014 field campaign were used to calibrate the

30   ice flow rate factor, A. The emergence rates across the ice cap were computed on a 200 m regular grid and scaled with the time span t_1-t_3, assuming constant emergence rate through the glaciological year. The calculated emergence rate $ch_{Ice\ dyn.}$icetools was then used for correcting the $dDEM_{t1}^{t3}$ at the in situ locations.

2) Assuming that the glacier is in a steady state, the long-term average surface net balance (divided by the density of ice) is equal in magnitude to the emergence rate across the glacier (Sold et al., 2013). Acknowledging that there is significant year-to-year variability in surface net mass balance, the net mass balance measurements from the year 2013-2014 were assumed to be representative of local emergence/submergence rates. Annual vertical velocities at the in situ locations were calculated using a density of 900 kg/m^3, and scaled by a factor 0.603 for representation of the velocities $ch_{Ice\ dyn.\mathrm{bn}}$ of the seven months period between t_1 and t_3.

4 Results

4.1 Uncertainty of satellite data

The statistics obtained from the dDEMs in snow-free and ice-free areas (Table 2) allow a quantitative comparison of the different methods and datasets used in the study. Statistics reveal significantly lower SD and NMAD when applying the filter of high slopes and shadow areas, while still retaining an adequate number of samples distributed over the majority of the study area (Table 2). This shows the dependency of the DEM accuracy with the steepness of the terrain (Toutin, 2002; Lacroix, 2016) and the presence of shadows. The remaining vertical bias obtained after DEM co-registration ranges from 0 to 0.1 m, based on median and trimmed mean of the statistics, and the NMAD reveals random errors <0.5 m in both schemes A and B as well as in the co-registered WV2 DEM, and both schemes reveal a strong similarity on the resulting elevation difference (dH) inside the ice cap.

The results obtained from SGSim provide estimate of the 95% uncertainty of the dDEM inside the ice cap. The SGSim results of both schemes coincide well to one another as well as within the uncertainty obtained from NMAD in the snow-free and ice-free areas. All proxies used show almost no bias in the dDEMs, especially for the scheme B, with virtually identical bias based on trimmed mean and SGSim (Table 2). This further supports the robustness of the two methods of DEM processing. However the results obtained from NMAD were kept as a conservative uncertainty of the dDEM, since the results obtained from SGSim can be slightly skewed by the presence of the thin layer of snow in the October 2014 images, affecting the data from presumed snow-free and ice-free areas, especially in close vicinity of the glacier. This may lead to an erroneous calculation of the bias inside the ice cap.

4.2 Maps of elevation differences and glacier-wide mass balance

Schemes A and B lead to similar elevation differences and uncertainty based on the statistical analysis (Table 2). Since it contains fewer data gaps, scheme B was used for producing the maps of elevation differences (Fig. 6) and for carrying out the study of volume changes and geodetic mass balance calculation.

The three dDEMs allow observing the temporal changes through the winter 2014-2015, revealing the pattern of snow accumulated on Drangajökull ice cap and surroundings (Fig. 6). The western half of the ice-cap exhibits larger amount of

elevation gain, with an average elevation difference dH = 5.74 m between October 2014 and May 2015, in comparison with the eastern half, dH = 5.20 m during the same period. Significant snow accumulation is also observed in several snowfields outside the ice cap. About two thirds of the total elevation gain within the ice cap boundary occurred between October 2014 and February 2015 (Table 3).

5   From (Eq. 1 and 2) the obtained glacier-wide winter mass balance is B_w = 3.20 ± 0.21 m. w.e. for the period 14 October 2014 – 22 May 2015. The mass balance obtained for the two periods of the winter was B = 1.92 ± 0.27 m. w.e. for the period 14 October 2014 to 13 February 2015 and B = 1.29 ± 0.34 m. w.e. for the period 13 February 2015 to 22 May 2015. Table 3 shows the summary of the mass balance and errors associated. It also quantifies the weight of each variable in the total error budget of the geodetic mass balance.

10   **4.3 Pléiades vs in situ data**

As expected, the in situ measurements of snow thickness yield substantially higher values than the difference in elevation measured from $dDEM_{t1}^{t3}$ in the accumulation area (Fig. 4), with an average difference of 2.56 m for points V3, V6, V7 and J2. In the ablation areas, however, the difference in elevation from $dDEM_{t1}^{t3}$ is larger than result from the in situ measurements (Fig. 4) with a difference of -0.98 m for Point V1. The areas closer to the ELA (points V2, V4 and V5, Fig. 1) show better

15   agreement between glaciological and remote sensing methods before applying corrections (Table 4).

The estimated corrections applied for calculating $\Delta dDEM_{t1}^{t3}$ are summarized in Table 4. Each correction has a different impact on the overall comparison, depending on the location of the in situ measurement. Highest corrections were estimated from ice dynamics deduced from the records of mass balance, $ch_{Ice\,dyn.\text{bn}}$, reaching up to 1.69 m of emergence at location V1. Corrections typically span from 0 to 1 meter (Table 4).

20   The estimated correction for the snowfall/ablation in the time difference between the beginning of winter and the first satellite acquisition, cht_{Oct}, assumes starting of the winter with the first snowfall, on the 3 of October 2014. However, records of temperature and MODIS images indicate likely melting of all the snow at the lowest location, V1, until the 13 October 2014. At this location, it was therefore assumed that the snowfall of 13 of October 2014 marked the beginning of the winter. Records of temperature suggest further melt at V1 after the October satellite acquisition. Since the degree day factor used is likely to

25   produce overestimates of this melt due to low sun angles, further correction of V1 was neglected for simplicity and inaccuracy of long term melting.

The mean difference between the in situ measurements and the obtained difference in elevation from $dDEM_{t1}^{t3}$ is 1.34 m (SD=1.43, N=8). The mean difference and its standard deviation are significantly reduced after applying the corrections, obtaining a mean difference of 0.40 m (SD=0.47) when calculating $\Delta dDEM_{t1}^{t3}$ using $ch_{Ice\,dyn.\text{icetools}}$ and a mean of 0.22 m

30   (SD=0.73) when calculating $\Delta dDEM_{t1}^{t3}$ using $ch_{Ice\,dyn.\text{bn}}$.

5 Discussion

5.1 Pléiades & WV DEMs for measuring snow accumulation

This study reveals accurately the mass balance evolution and snow distribution through one winter period for an entire ice cap entirely from remote sensing. This technique can be applied in small and medium size glaciated areas (>5000 km^2 can be

5   stereoscopically covered at once based on the capabilities of Pléiades and WV2), with sufficiently high mass turnover (~0.5-1 m w.e. or higher). The satellite stereo images have as main advantages the repeatability and the access to remote glaciated areas. The use of external reference data, such as lidar-based or GPS-based GCPs, does not improve the relative accuracy of the dDEMs (Table 2).

Combining data from Pléiades and WorldView, allows for high spatial resolution within a short 3-4 month interval. The

10   availability of these data and the presented processing strategy allow, to our knowledge, for the first satellite-based measurement of winter accumulation on a glacier. Both sensors present a similar level of accuracy and other comparable characteristics, so that their combination enables more detailed studies of glacier changes.

The two methodologies carried out for DEM processing have pros and cons. Scheme A has the advantage of obtaining all results (DEMs, orthoimages, dDEMs) in a well-known reference system, based on a geodetic network where the lidar DEM is

15   fixed (or similar if GPS-based GCPs are used). It is also adequate when limited unchanged areas are available, if there are identifiable features for extraction of GCPs. This approach, however, requires external spatial information and the tedious process of manual GCP selection. On the positive side, scheme B uses a highly automated workflow and it is independent of spatial information other than the satellite images and camera model information, providing as well less amount of data gaps. But scheme B is dependent on the availability of spatially well-distributed unchanged areas for co-registration (Shean et al.,

20   2016).

The ice cap wide geodetic mass balances suggest that ~60% of the winter accumulation was deposited in the first 4 months of the winter (14 October 2014 – 13 February 2015, Table 3 and Fig. 6). Precipitation records at a weather station, ~40 km from the glacier, indicate the same ratio of accumulation for the two time periods, 342 mm (62% of total) between 14 October 2014 and 13 February 2015, and 218 mm (38% of total) between 13 February 2015 and 22 of May 2015 (Fig. 5). The consistency

25   of the ratio of accumulation in the two sub-periods observed at the weather station and calculated from the satellite images also supports the applicability of the corrections applied due to mismatch in time between in situ and geodetic mass balance observations.

5.2 Snow density and firn compaction in calculation of sub-annual geodetic mass balance

The snow density and firn compaction are needed to retrieve the glacier-wide geodetic mass balance (Eq. 1) and are estimated

30   based on in situ data acquired from the ongoing Icelandic glacier monitoring program. Ice dynamics do not affect the calculation of glacier-wide geodetic mass balance due to the principle of mass conservation (Cuffey and Paterson, 2010).

The sensitivity of the mass balance calculation was tested using different snow densities measured during 2005-2014 field campaigns in Drangajökull (Fig. 7). The glacier-wide winter mass balance is reduced by 1% when the average of all previous density records are used instead of the mean 2015 density. Using the minimum average density recorded, 511 kg/m^3 in 2011, resulted in 8% lower mass balance, and using the maximum average density recorded, 583 kg/m^3 in 2008, resulted in a 5% higher mass balance.

Snow density records from other Icelandic ice caps were also used for testing this sensitivity. The average density measured on Mýrdalsjökull ice cap in 2010 (Ágústsson et al., 2013), and the average density measured on Langjökull ice cap in 2015, produced 3% and 10% overestimation and underestimation of mass balance, respectively.

These results show that the geodetic mass balance during a winter period is sensitive to the snow density used, and how snow density from different glaciers or from different years in the same area can vary substantially. However the relatively low scatter of density distribution over the different in situ locations on Drangajökul (Fig. 7) indicate that the density measurements of one or a few points at a close date to the satellite acquisitions would give reasonable results for the geodetic glacier-wide mass balance calculations.

The estimated effect of firn compaction in this study adds 4% to the derived geodetic mass balance (Table 3). The approach used for firn correction assumes a constant annual mass balance in the accumulation area, which is a significant source of uncertainty due to high interannual climate variability. Other methods can be used for this correction, such as deep core drilling (Thorsteinsson et al., 2002), or more robust firn layer observations and modelling (e.g. Sold et al., 2015).

Additionally, these elevation change maps will aid in selection of representative locations for in situ measurements. Obtaining both glaciological and geodetic data at the same or close dates will lead to an accurate glacier-wide mass balance with only a few density measurements and previous records of mass balance. Remote areas without information of snow density or firn compaction can also be studied from remote sensing, allowing obtaining estimates of geodetic mass balance with error bars ranging between 5% and 10% for glaciers with mass turnover similar to Drangajökull. The error in geodetic mass balance is primary associated with physical parameters of the glacier (snow density and firn compaction) and, to a lesser extent, to the ability to derive map of elevation differences from satellite data (Table 3).

5.3 Remote sensing vs in situ

The comparison of elevation differences measured from Pléiades (geodetic method) and the snow thickness measured in situ (glaciological method) is not straightforward and it requires familiarity with the glacier's dynamics to adequately interpret the difference between the two types of measurements.

The points V1-V4 are located at Leirufjarðarjökull (Fig. 1), a surge-type glacier (Björnsson et al., 2003; Brynjólfsson et al., 2016). The dynamics of this glacier outlet are by nature not in balance with the rate of accumulation or ablation, and thus the approach (2), i.e. using the net annual mass balance average over multiple years, for calculation of vertical velocities may be inappropriate at these locations. On the other hand, it is observed an underestimation of submergence velocities in the southern areas using approach (1) for ice dynamics, possibly explained by the lack of basal sliding in the ice flow model. Only minor

elevation changes have been detected in this part of the glacier in the past decades (Magnússon et al., 2016), and it is not known to surge, hence the approach (2) may be more suitable at these locations.

The temporal offset between glaciological and geodetic measurements results in some ambiguity in the definition of the beginning and the end of the balance season. Glaciological measurements generally use the previous summer layer as reference, which ensures a well-defined starting point of the balance year, despite the fact that the date chosen for the spring campaign (i.e. the winter balance end date) is not so objectively defined. For example, two snow events occurred in late May and early June, which can either be considered part of the winter or summer balance seasons. The timing of remote sensing surveys are further dependent on sensor tasking and favorable weather (cloud-free) conditions and, as a consequence, a temporal offset between glaciological and geodetic observations is likely. Logistics in fieldwork and scheduling satellite acquisition can improve the agreement of the results if there is a reduced temporal difference between in situ and remote sensing data.

6 Conclusions

This study indicates that the DEMs created from satellite stereo images Pléiades and WV2 can be used for measuring changes in elevation in glaciers in seasonal time spans. Relative accuracy of 20-30 cm allowed measuring the evolution of snow accumulation in two periods of the winter on Drangajökull ice cap. Two methodologies used for the processing of DEMs yielded similar accuracy and elevation changes with and without using GCPs, showing that the processing of satellite stereo images for measuring glacier evolution can be performed without external reference data for GCP extraction, such as lidar or GPS data.

The records of glacier-wide mass balance were calculated by geodetic means on sub-annual time scales, with uncertainty ranging between 0.2 and 0.4 m w.e. The period 14 October 2014 – 22 May 2015 shows $B_w = 3.20 \pm 0.21$ m w.e., and ~60% of the accumulation happened during the period 14 October 2014 – 13 February 2015. This calculation required information about the snow density for volume to water equivalent conversion, and knowledge of the rate of firn compaction, estimated from in situ measurements. The uncertainty in the snow density has the largest contribution to the uncertainty in B_w, significantly larger than the uncertainty in the average elevation change and the firn compaction.

The firn compaction estimate added 4% to the mass balance obtained from the geodetic method, and this contribution in geodetic mass balance is dependent on the amount of winter snow typically left on the glacier in the autumn in recent years. The inaccuracy of sub annual geodetic mass balance can be minimized with records of snow density and previous years' mass balance. It can however lead to significant errors if density measurements are extrapolated from other glaciers with different characteristics.

The satellite-derived map of elevation difference was analyzed and compared to eight in situ measurements. An appropriate comparison of the two types of measurements requires a good understanding of three phenomena leading to sub-meter and meter-level elevation changes. These phenomena are: (1) The difference in time between in situ campaigns and satellite

acquisitions, (2) the effect of firn compaction in the accumulation area and (3) the vertical component of the ice flow motion. In this case study, these three phenomena have a similar order of magnitude.

The presented method provides possibilities for glacier mass balance monitoring on sub-annual time scales from remote sensing data, due to the rapid increase and availability of optical satellites collecting stereo images in glaciated regions with dense temporal resolution. It allows obtaining fair estimates of the glacier-wide seasonal mass balance in areas where expected mean thickness of winter snow exceeds 1 m. The accuracy of such studies is however improved significantly when geodetic data and in situ information are combined.

Acknowledgements. This study was funded by the University of Iceland Research Fund. Pléiades images were acquired at research price thanks to the CNES ISIS program (http://www.isis-cnes.fr). The WV2 DEM was obtained as a part of the ArcticDEM project. This work is a contribution to the Rannís grant of excellence project, ANATILS. Collaboration and travels between IES and LEGOS were funded by the Jules Verne research fund and the TOSCA program from CNES. This study used the recent lidar mapping of the glaciers in Iceland that was funded by the Icelandic Research Fund, the Landsvirkjun Research Fund, the Icelandic Road Administration, the Reykjavík Energy Environmental and Energy Research Fund, the Klima- og Luftgruppen (KoL) research fund of the Nordic Council of Ministers, the Vatnajökull National Park, the organization Friends of Vatnajökull, the National Land Survey of Iceland and the Icelandic Meteorological Office. The ground-based mass balance measurements on Drangajökull have been jointly funded by Orkubú Vestfjarða (Westfjord Power Company), National Energy Authority (2004-2009) and the Icelandic Meteorological Office (2009-2015).

References

Adalgeirsdóttir, G., Gudmundsson, S., Björnsson, H., Pálsson, F., Jóhannesson, T., Hannesdóttir, H., Sigurdsson, S. Þ. and Berthier, E.: Modelling the 20th and 21st century evolution of Hoffellsjökull glacier, SE-Vatnajökull, Iceland, The Cryosphere, 5(4), 961–975, doi:10.5194/tc-5-961-2011, 2011.

Ágústsson, H., Hannesdóttir, H., Thorsteinsson, T., Pálsson, F. and Oddsson, B.: Mass balance of Mýrdalsjokull ice cap accumulation area and comparison of observed winter balance with simulated precipitation, Jokull, 63, 91–104, 2013.

Berthier, E., Vincent, C., Magnússon, E., Gunnlaugsson, Á. Þ., Pitte, P., Le Meur, E., Masiokas, M., Ruiz, L., Pálsson, F., Belart, J. M. C. and Wagnon, P.: Glacier topography and elevation changes derived from Pléiades sub-meter stereo images, The Cryosphere, 8(6), 2275–2291, doi:10.5194/tc-8-2275-2014, 2014.

Björnsson, H. and Pálsson, F.: Icelandic glaciers, Jokull, 58, 365–386, 2008.

Björnsson, H., Pálsson, F., Sigurdsson, O. and Flowers, G. E.: Surges of glaciers in Iceland, Ann. Glaciol. Vol 36, 82–90, 2003.

Björnsson, H., Pálsson, F., Guðmundsson, S., Magnússon, E., Aðalgeirsdóttir, G., Jóhannesson, T., Berthier, E., Sigurðsson, O. and Thorsteinsson, T.: Contribution of Icelandic ice caps to sea level rise: trends and variability since the Little Ice Age, Geophys. Res. Lett., 40, 1–5, doi:10.1002/grl.50278, 2013.

Brynjólfsson, S., Schomacker, A., Korsgaard, N. J. and Ingólfsson, Ó.: Surges of outlet glaciers from the Drangajökull ice cap, northwest Iceland, Earth Planet. Sci. Lett., 450, 140–151, doi:10.1016/j.epsl.2016.06.039, 2016.

Bühler, Y., Adams, M. S., Bösch, R. and Stoffel, A.: Mapping snow depth in alpine terrain with unmanned aerial systems (UASs): potential and limitations, The Cryosphere, 10(3), 1075–1088, doi:10.5194/tc-10-1075-2016, 2016.

5   Cuffey, K. M. and Paterson, W. S. B.: The physics of glaciers, Academic Press Inc, Amsterdam., 2010.

De Michele, C., Avanzi, F., Passoni, D., Barzaghi, R., Pinto, L., Dosso, P., Ghezzi, A., Gianatti, R. and Della Vedova, G.: Using a fixed-wing UAS to map snow depth distribution: an evaluation at peak accumulation, The Cryosphere, 10(2), 511–522, doi:10.5194/tc-10-511-2016, 2016.

Guðmundsson, M. T.: Mass balance and precipitation on the summit plateau of Oraefajokull, SE-Iceland, , 48, 49–54, 2000.

10   Guðmundsson, S., Björnsson, H., Pálsson, F. and Haraldsson, H. H.: Comparison of energy balance and degree-day models of summer ablation on the Langjokull ice cap, SW-Iceland, Jokull, 59, 1–18, 2009.

Helfricht, K., Kuhn, M., Keuschnig, M. and Heilig, A.: Lidar snow cover studies on glaciers in the Ötztal Alps (Austria): comparison with snow depths calculated from GPR measurements, The Cryosphere, 8(1), 41–57, doi:10.5194/tc-8-41-2014, 2014.

15   Höhle, J. and Höhle, M.: Accuracy assessment of digital elevation models by means of robust statistical methods, ISPRS J. Photogramm. Remote Sens., 64(4), 398–406, doi:10.1016/j.isprsjprs.2009.02.003, 2009.

Holzer, N., Vijay, S., Yao, T., Xu, B., Buchroithner, M. and Bolch, T.: Four decades of glacier variations at Muztagh Ata (eastern Pamir): a multi-sensor study including Hexagon KH-9 and Pléiades data, The Cryosphere, 9(6), 2071–2088, doi:10.5194/tc-9-2071-2015, 2015.

20   Howat, I. M., Porter, C., Noh, M. J., Smith, B. E. and Jeong, S.: Brief Communication: Sudden drainage of a subglacial lake beneath the Greenland Ice Sheet, The Cryosphere, 9(1), 103–108, doi:10.5194/tc-9-103-2015, 2015.

Huss, M., Bauder, A., Funk, M. and Hock, R.: Determination of the seasonal mass balance of four Alpine glaciers since 1865, J. Geophys. Res.-Earth Surf., 113(F1), 2008.

James, T. D., Murray, T., Barrand, N. E. and Barr, S. L.: Extracting photogrammetric ground control from lidar DEMs for 25   change detection, Photogramm. Rec., 21(116), 312–328, 2006.

Jarosch, A. H.: Icetools: A full Stokes finite element model for glaciers, Comput. Geosci., 34(8), 1005–1014, doi:10.1016/j.cageo.2007.06.012, 2008.

Jóhannesson, T., Björnsson, H., Pálsson, F., Sigurðsson, O. and Þorsteinsson, Þ.: LiDAR mapping of the Snæfellsjökull ice cap, western Iceland, Jökull, 61, 19–32, 2011.

30   Jóhannesson, T., Björnsson, H., Magnússon, E., Guðmundsson, S., Pálsson, F., Sigurðsson, O., Thorsteinsson, T. and Berthier, E.: Ice-volume changes, bias estimation of mass-balance measurements and changes in subglacial lakes derived by lidar mapping of the surface of Icelandic glaciers, Ann. Glaciol., 54(63), 63–74, doi:10.3189/2013AoG63A422, 2013.

Lacroix, P.: Landslides triggered by the Gorkha earthquake in the Langtang valley, volumes and initiation processes, Earth Planets Space, 68(1), 46, doi:10.1186/s40623-016-0423-3, 2016.

Lacroix, P., Berthier, E. and Maquerhua, E. T.: Earthquake-driven acceleration of slow-moving landslides in the Colca valley, Peru, detected from Pléiades images, Remote Sens. Environ., 165, 148–158, doi:10.1016/j.rse.2015.05.010, 2015.

Magnússon, E., Belart, J. M. C., Pálsson, F., Ágústsson, H. and Crochet, P.: Geodetic mass balance record with rigorous uncertainty estimates deduced from aerial photographs and lidar data – Case study from Drangajökull ice cap, NW Iceland, The Cryosphere, 10(1), 159–177, doi:10.5194/tc-10-159-2016, 2016.

Marti, R., Gascoin, S., Berthier, E., de Pinel, M., Houet, T. and Laffly, D.: Mapping snow depth in open alpine terrain from stereo satellite imagery, The Cryosphere, 10(4), 1361–1380, doi:10.5194/tc-10-1361-2016, 2016.

Noh, M.-J. and Howat, I. M.: Automated stereo-photogrammetric DEM generation at high latitudes: Surface Extraction with TIN-based Search-space Minimization (SETSM) validation and demonstration over glaciated regions, GIScience Remote Sens., 52(2), 198–217, doi:10.1080/15481603.2015.1008621, 2015.

Nuth, C. and Kääb, A.: Co-registration and bias corrections of satellite elevation data sets for quantifying glacier thickness change, The Cryosphere, 5(1), 271–290, doi:10.5194/tcd-4-2013-2010, 2011.

Ohmura, A.: Observed Mass Balance of Mountain Glaciers and Greenland Ice Sheet in the 20th Century and the Present Trends, Surv. Geophys., 32(4–5), 537–554, 2011.

Pálsson, F., Guðmundsson, S., Björnsson, H., Berthier, E., Magnússon, E., Guðmundsson, S. and Haraldsson, H.: Mass and volume changes of Langjökull ice cap, Iceland, ~1890 to 2009, deduced from old maps, satellite images and in situ mass balance measurements, Jökull, 62, 81–96, 2012.

Pomerleau, F., Colas, F., Siegwart, R. and Magnenat, S.: Comparing ICP variants on real-world data sets, Auton. Robots, 34(3), 133–148, doi:10.1007/s10514-013-9327-2, 2013.

Rolstad, C., Haug, T. and Denby, B.: Spatially integrated geodetic glacier mass balance and its uncertainty based on geostatistical analysis: application to the western Svartisen ice cap, Norway, J. Glaciol., 55(192), 666–680, 2009.

Shean, D. E., Alexandrov, O., Moratto, Z. M., Smith, B. E., Joughin, I. R., Porter, C. and Morin, P.: An automated, open-source pipeline for mass production of digital elevation models (DEMs) from very-high-resolution commercial stereo satellite imagery, ISPRS J. Photogramm. Remote Sens., 116, 101–117, doi:10.1016/j.isprsjprs.2016.03.012, 2016.

Sold, L., Huss, M., Hoelzle, M., Andereggen, H., Joerg, P. C. and Zemp, M.: Methodological approaches to infer end-of-winter snow distribution on alpine glaciers, J. Glaciol., 59(218), 1047–1059, doi:10.3189/2013JoG13J015, 2013.

Sold, L., Huss, M., Eichler, A., Schwikowski, M. and Hoelzle, M.: Unlocking annual firn layer water equivalents from ground-penetrating radar data on an Alpine glacier, The Cryosphere, 9(3), 1075–1087, doi:10.5194/tc-9-1075-2015, 2015.

Tarini, M., Cignoni, P. and Montani, C.: Ambient Occlusion and Edge Cueing for Enhancing Real Time Molecular Visualization, IEEE Trans. Vis. Comput. Graph., 12(5), 1237–1244, doi:10.1109/TVCG.2006.115, 2006.

Thorsteinsson, T., Sigurðsson, O., Jóhannesson, T., Larsen, G. and Wilhelms, F.: Ice core drilling on the Hofsjökull ice cap, Jökull, 51, 25–41, 2002.

Toutin, T.: Three-dimensional topographic mapping with ASTER stereo data in rugged topography, IEEE Trans. Geosci. Remote Sens., 40(10), 2241–2247, doi:10.1109/TGRS.2002.802878, 2002.

Vaughan, D. G., Comiso, J. C., Allison, J., Carrasco, J., Kaser, R., Kwok, R., Mote, P., Murray, T., Paul, F., Ren, J., Rignot, E., Solomina, O., Steffen, K. and Zhang, T.: Observations: Cryosphere, in Climate Change 2013: The Physical Science Basis. Contribution of Working Group I to the Fifth Assessment Report of the Intergovernmental Panel on Climate Change, Cambridge University Press, Cambridge, United Kingdom and New York, NY, USA., 2013.

5   Willis, M. J., Herried, B. G., Bevis, M. G. and Bell, R. E.: Recharge of a subglacial lake by surface meltwater in northeast Greenland, Nature, 518(7538), 223–227, 2015.

Zemp, M., Frey, H., Gärtner-Roer, I., Nussbaumer, S. U., Hoelzle, M., Paul, F., Haeberli, W., Denzinger, F., Ahlstrøm, A. P., Anderson, B., Bajracharya, S., Baroni, C., Braun, L. N., Cáceres, B. E., Casassa, G., Cobos, G., Dávila, L. R., Delgado Granados, H., Demuth, M. N., Espizua, L., Fischer, A., Fujita, K., Gadek, B., Ghazanfar, A., Hagen, J. O., Holmlund, P.,
10 Karimi, N., Li, Z., Pelto, M., Pitte, P., Popovnin, V. V., Portocarrero, C. A., Prinz, R., Sangewar, C. V., Severskiy, I., Sigurðsson, O., Soruco, A., Usubaliev, R. and Vincent, C.: Historically unprecedented global glacier decline in the early 21st century, J. Glaciol., 61(228), 745–762, doi:10.3189/2015JoG15J017, 2015.

Table 1: Dates, type of data (split in remote sensing and in situ data), sampling and specifications of datasets used in this study.

	Date	Data Type	Spatial Resolution	Comments
REMOTE SENSING	20 Jul 2011	Lidar DEM	2 x 2 m cell size	
	14 Oct 2014	Pléiades stereo	0.70 m pixel size	B/H 0.48
	13 Feb 2015	WV2 SETSM DEM & Ortho	2 x 2 m cell size	B/H 0.45
	22 May 2015	Pléiades stereo	0.70 m pixel size	B/H 0.41
IN SITU	Springs 2005 - 2015	Snow density	6 to 12 points	Spring 2013 missing due to bad weather
	1 Jan 2014 – 2015 31 Dec 2015	Daily Precipitation & Temperature		Litla Ávík
	Spring 2014 & Autumn 2014	Net Mass Balance	12 points + interpolated net balance map	Spring 2014: Shallow cores & GPR profiles. Autumn 2014: Ablation stakes.
	19 Jun 2015	Winter Mass Balance	8 points	

Table 2: Uncertainty analysis in snow-free and ice-free areas of the dDEMs, and mean elevation difference inside the ice cap, dH. N represents number of data points. Trim mean excludes 5% of the data at each tail of the histogram. The three bottom rows indicate the statistics after masking slopes >20° and shadows. Bias-corrected SGSim represents the mean elevation bias from 1000 simulations and the standard deviation of the simulations (details in Magnússon et al., 2016).

	Scheme	N (x10⁶)	Gaps icecap (%)	Mean (m)	Median (m)	Trim Mean (m)	SD (m)	NMAD (m)	Mean dH (m)	Bias-corrected SGSim (m)
Raw snow- ice-free	A - Lidar GCPs	2.2	3.9%	-0.16	-0.10	-0.15	1.12	0.48	5.40	-
	B – ICP	2.6	0.8%	0.00	0.02	-0.01	1.36	0.35	5.53	-
	WV2 ICP	2.4	8.2%	0.04	0.00	0.03	1.26	0.50	3.72	-
Slopes & shadows mask	A - Lidar GCPs	1.4	6.2%	-0.08	-0.05	-0.08	0.49	0.35	5.36	5.61 ± 0.10
	B –ICP	1.5	2.4%	-0.02	0.02	-0.01	0.54	0.22	5.56	5.55 ± 0.08
	WV2 ICP	0.9	10.4%	0.04	0.02	0.03	0.39	0.34	3.71	-

Table 3: Geodetic mass balance and associated error. Δ indicates uncertainty of each variable affecting the geodetic mass balance B. ΔB_ρ, $\Delta B_{\bar{h}_{dDEM}}$ and $\Delta B_{\overline{ch}_{Firn}}$ show the contribution of the density, elevation difference and firn correction respectively, to the total uncertainty ΔB, which is computed as the quadratic sum of the three variables.

| | $\bar{h}_{dDEM}$ | $\overline{ch}_{Firn}$ | ρ | Δ_ρ | ΔB_ρ | $\Delta_{\bar{h}_{dDEM}}$ | $\Delta B_{\bar{h}_{dDEM}}$ | $\Delta_{\overline{ch}_{Firn}}$ | $\Delta B_{\overline{ch}_{Firn}}$ | B | ΔB |
	(m)	(m)	(kg/m³)	(kg/m³)	(m. w.e.)	(m)	(m. w.e.)	(m)	(m. w.e.)	(m. w.e.)	(m. w.e.)
t_1^3	5.54	0.24	554	30	0.16	0.22	0.12	0.12	0.07	3.20	0.21
t_1^2	3.72	0.13	500	50	0.19	0.34	0.19	0.07	0.04	1.92	0.27

Table 4: Comparison of values of snow thickness obtained in situ and elevation difference obtained from Pléiades DEMs. The table lists all corrections applied to the Pleiades elevation differences to make them comparable to the in situ measurements (see text for details). The table also compares two approaches carried out for correction of ice motion: (1) using the glacier ice flow model (Jarosch, 2008) and (2) using records of mass balance (Sold et al., 2013). $C_1 dDEM_{t1}^{t3}$ and $C_2 dDEM_{t1}^{t3}$ are the resulting corrections of the dDEM using the two different approaches, and Res_1 and Res_2 are the remaining differences between the glaciological and geodetic methods after applying the corrections.

	$B_{W\ in-situ}$	$dDEM_{t1}^{t3}$	cht_{Oct}	$cht_{May\&Jun}$	ch_{Firn}	$ch_{Ice\ dyn.icetools}$	$C_1 dDEM_{t1}^{t3}$	Res_1	$ch_{Ice\ dyn.bn}$	$C_2 dDEM_{t1}^{t3}$	Res_2
	(m)	(m)	(m)	(m)	(m)	(m)	(m)	(m)	(m)	(m)	(m)
V1	2.90	3.88	0.13	-0.95	0.00	-0.51	2.55	0.35	-1.69	1.37	1.53
V2	5.63	5.34	0.27	-0.16	0.00	-0.50	4.95	0.68	-0.88	4.56	1.07
V3	8.38	5.86	0.84	0.37	0.58	0.10	7.75	0.63	1.16	8.81	-0.43
V4	4.95	4.18	0.63	0.23	0.13	0.21	5.38	-0.43	0.25	5.42	-0.47
V5	5.68	5.32	0.34	0.02	0.00	-0.09	5.60	0.08	-0.07	5.62	0.06
V6	8.60	5.67	0.80	0.41	0.50	0.02	7.40	1.20	1.00	8.38	0.22
V7	8.09	5.21	0.92	0.45	0.44	0.70	7.72	0.37	0.88	7.91	0.18
J2	7.60	5.67	0.78	0.32	0.41	0.12	7.30	0.30	0.81	7.98	-0.38
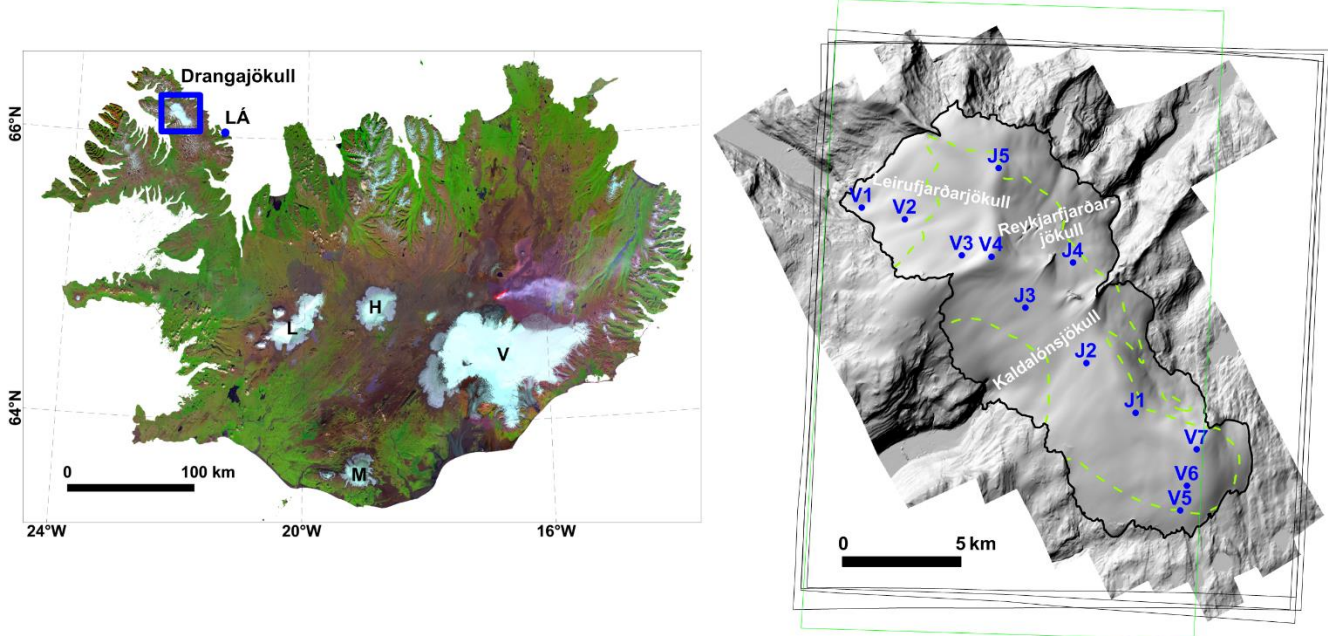
Figure 1: Area of study and data collected. Left: Mosaic of Iceland from Landsat 8 images, courtesy of the National Land Survey of Iceland. The blue rectangle locates Drangajökull ice cap, and a blue dot indicates location of the meteorological station "Littla Ávík" (LÁ). L, M, V and H represent locations of Langjökull, Mýrdalsjökull, Vatnajökull and Hofsjökull ice caps, respectively. Right: A shaded relief representation of a lidar DEM covering Drangajökull and vicinity in the summer 2011 (Jóhannesson et al., 2013). Margins of the ice cap are shown with a black polygon, and the equilibrium line altitude (ELA) is shown with a green dashed line. Blue dots indicate location of the in situ measurements. Locations labelled Vx have been measured since 2005, whereas locations labelled Jx were only measured in 2014 except J2, which was also measured in 2015. Black rectangles show the footprints of the Pléiades images, and a green rectangle shows the footprint of the WV2 DEM.
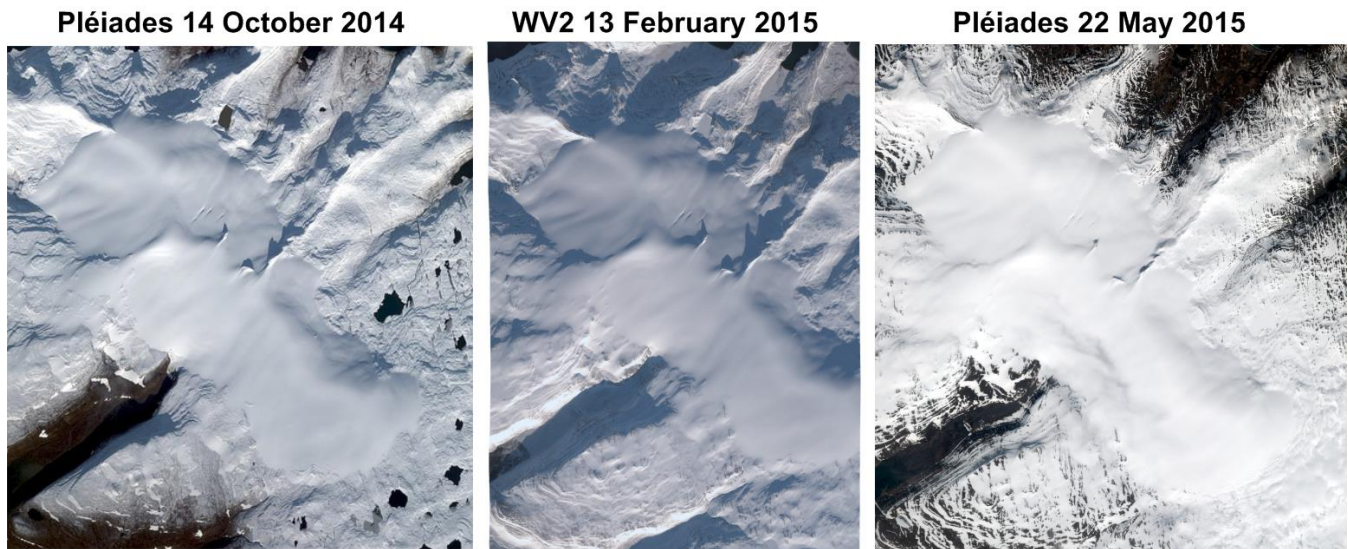
Figure 2: Quickviews of the satellite images. Left image from each stereo pair is shown. © CNES 2014 and 2015, Airbus D&S, All copyrights reserved (Pléiades) and © DigitalGlobe (WV2). Quickviews downloadable at: http://www.intelligence-airbusds.com/en/4871-browse-and-order (Pléiades) and https://browse.digitalglobe.com (WV2).
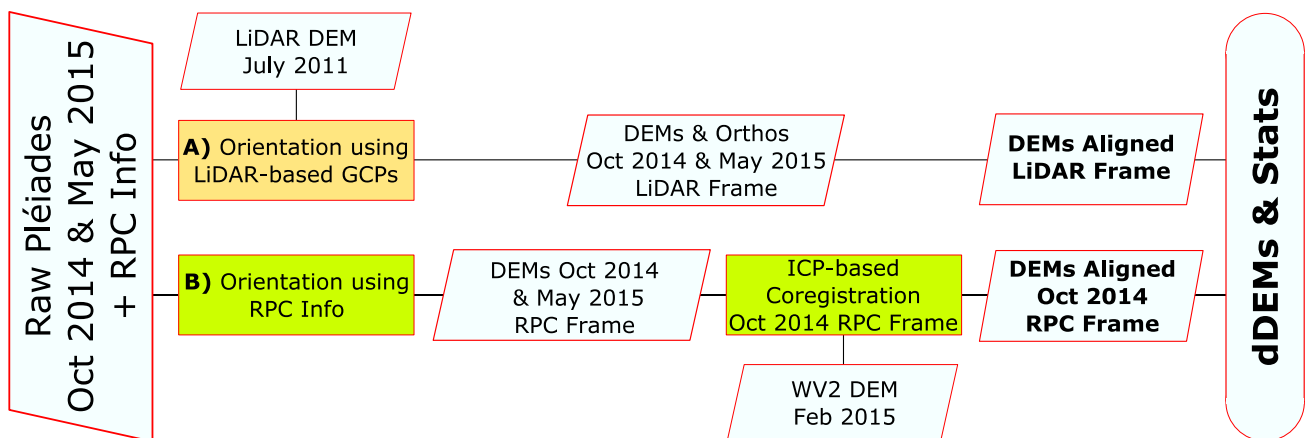
Figure 3: Flowchart of the different schemes studied for obtaining unbiased DEMs. Orange squares indicate processing with ERDAS software, and green squares indicate processing with ASP software.
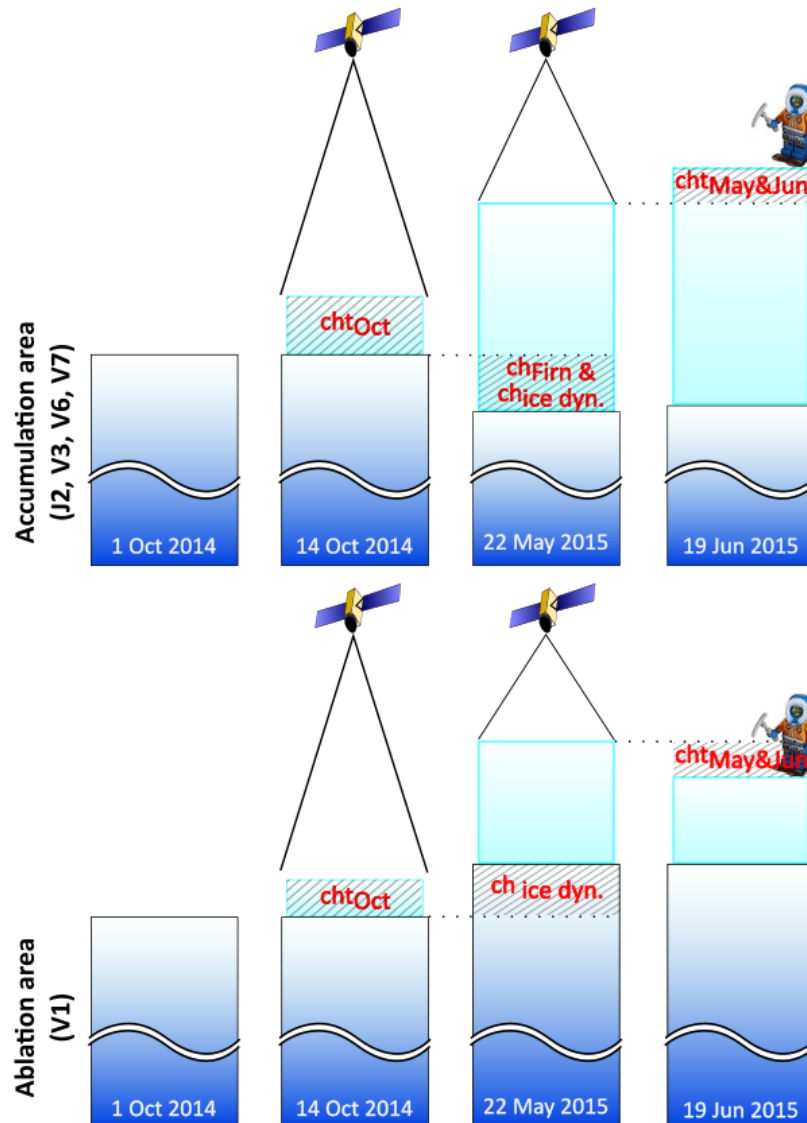
Figure 4: Sketch of the different factors affecting the comparison between the glaciological (1 Oct 2014 – 19 Jun 2015) and geodetic (14 Oct 2014 – 22 May 2015) methods. Light blue represents snow fallen in winter, and dark blue represents pre-existing ice and firn.
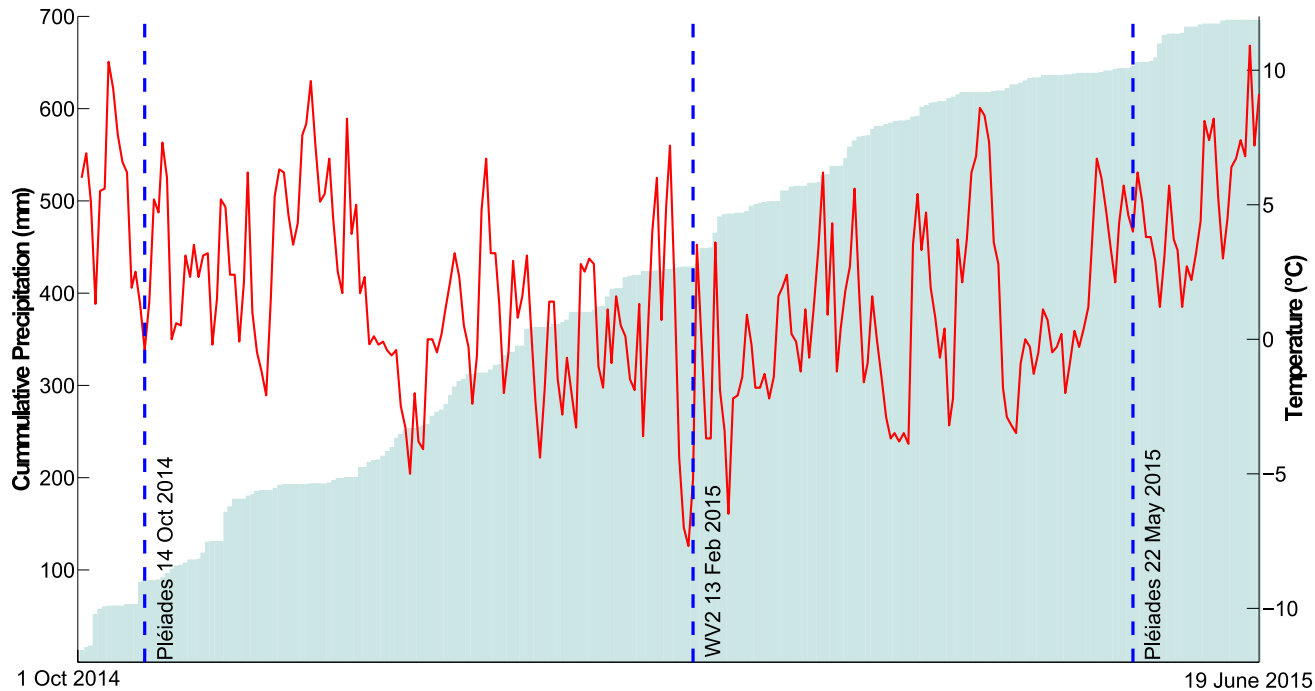
Figure 5: Cumulative precipitation (clear blue) and temperature (red line) for the winter 2014-2015 (1 October 2014 to 19 June 2015) from the station Litla Ávík. Blue dashed lines show the time of acquisition of satellite stereo images.
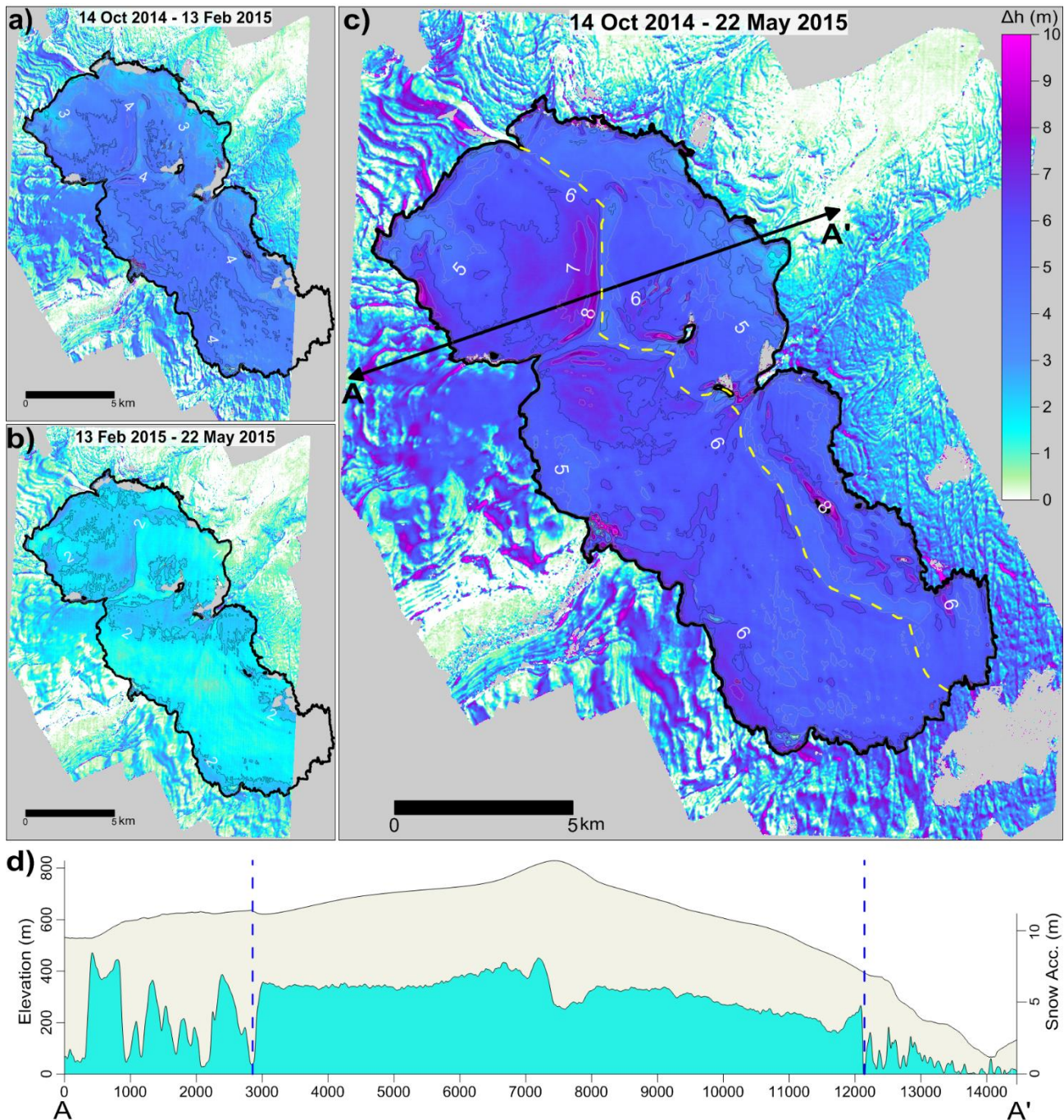
Figure 6: Elevation difference based on Pléiades and WV2 data. a) Elevation difference from October 2014 (Pléiades) to February 2015 (WV2). b) Elevation difference from February 2015 (WV2) to May 2015 (Pléiades). c) Elevation difference from October 2014 (Pléiades) to May 2015 (Pléiades). A black polygon indicates the glacier margin in October 2014. Yellow dashed line shows the
5 **boundary between eastern and western halves of the ice cap. Contours inside the ice cap have been smoothed with a Gaussian filter of 19x19 windows size. d) Longitudinal profile A-A' with surface elevation (beige) and snow thickness (blue) over the glacier and ice-free areas. The blue dashed lines indicate the locations of the glacier margins.**
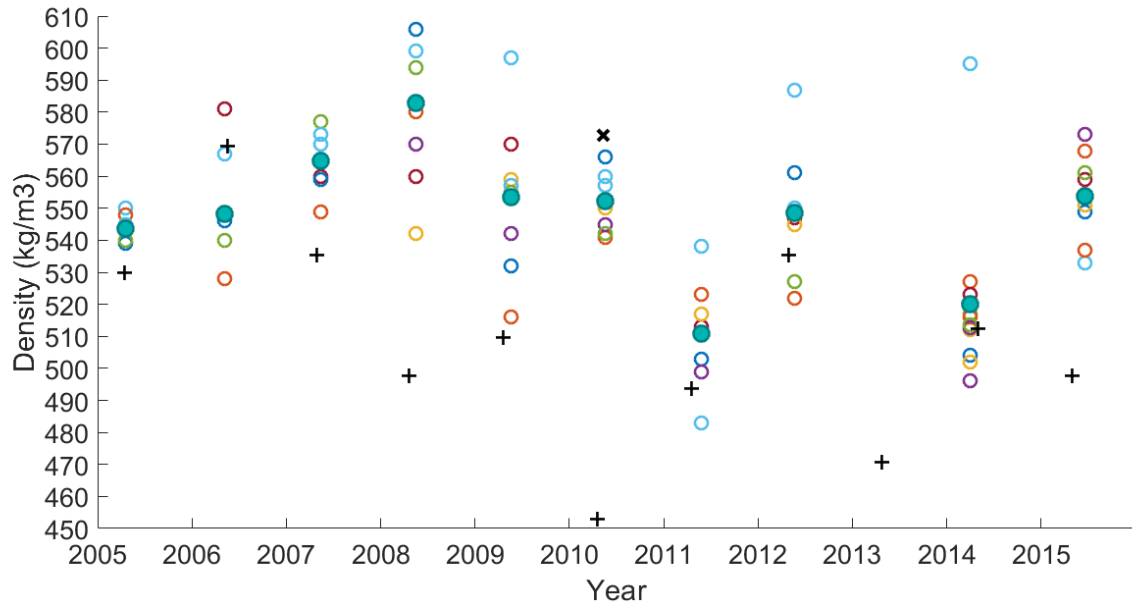
Figure 7: The density values obtained at each in situ location for field campaigns 2005-2015. Each circle represents the average density of the shallow core at each in situ location. Blue filled circles show the average annual density measurements. Black "+" shows the averaged density measured on Langjökull, and black "X" shows the averaged density measured on Mýrdalsjökull ice cap in year 2010 (Ágústsson et al., 2013). The 2013 campaign was not carried out due to bad weather conditions.